Theoretical aspects of intense field harmonic generation

## TOPICAL REVIEW

# Theoretical aspects of intense field harmonic generation

Anne L'Huillier†, Kenneth J Schafer‡ and Kenneth C Kulander‡

† DRECAM, Service des Photons, Atomes et Molécules, Bâtiment 522, Centre d'Etudes de Saclay, 91191 Gif-sur-Yvette, France
‡ Lawrence Livermore National Laboratory, Physics Department, PO Box 808, Livermore, CA, USA

**Abstract.** We present theoretical studies of high-order harmonic generation in a rare-gas medium. The experimental results obtained at Saclay with a 1064 nm Nd-YAG laser in the $10^{13}$ W cm$^{-2}$ intensity range are summarized. The harmonic emission strengths first decrease rather steeply for the first orders, then form a long plateau up to the 21st harmonic in xenon, or up to the 33rd harmonic in argon, before decreasing again rather abruptly. The theoretical description of these experiments consists first in the calculation of the photo-emission spectra emitted by a single atom. The spectra are obtained by numerically integrating a time-dependent Schrödinger equation for the laser-excited rare-gas atom. Second, one must account for collective effects in the medium, described by Maxwell's equations. A theoretical framework for describing the generation and propagation of harmonics in strong laser fields is developed. A numerical solution of the propagation equations for the harmonic fields in xenon at 1064 nm provides results which agree well with experimental data. We discuss the role of phase matching in the high-order harmonic generation experiments. The main conclusion is that phase matching is determined not only by the variation of the phases of the interfering fields in the non-linear medium, but also by the variation of the amplitudes throughout the medium. We find orders of magnitude improvement in phase matching in a strong-field regime compared with the perturbative limit.

## 1. Introduction

An intense laser focused into a 10 Torr rare-gas vapour leads to the generation of very high-order odd harmonics of the pump field. Experiments performed at the University of Illinois at Chicago (McPherson *et al* 1987, Rosman *et al* 1988) showed the generation of up to the 17th harmonic of a 248 nm KrF laser in a neon vapour. The 33rd harmonic in argon and the 21st harmonic in xenon have been observed at Saclay using a 1064 nm Nd-YAG laser (Ferray *et al* 1988, Li *et al* 1989). This was recently extended to the 25th harmonic of a KrF laser by Sarukura *et al* (1991) and to the 53rd harmonic of a 1 ps 1053 nm Nd-glass laser by L'Huillier *et al* (1991a), both produced in a neon vapour. These experiments performed with short pulses and at high laser intensities result in very short wavelength coherent radiation, 10 nm (125 eV) for the 25th harmonic of a 248 nm laser, 20 nm (62 eV) for the 53rd harmonic of a 1053 nm laser. Efficiencies are of the order of $10^{-11}$–$10^{-9}$. These frequency conversion processes might lead to useful sources of short pulse, short wavelength coherent radiation. They seem to be much more promising than previous experimental investigations performed with longer pulse infrared lasers (Metchkov *et al* 1977, Groseva *et al* 1977, Wildenauer 1987) or ultraviolet pump fields (Reintjes *et al* 1978, 1981, Bokor *et al* 1983) which were limited by various effects such as the ionization of the medium, the absorption of the generated radiation in optically thick media and/or the breakdown of phase-matching conditions.

The harmonic intensities in the strong-field regime exhibit a characteristic distribution. After the expected rapid decrease for the first orders, there is a long plateau,

which ends up with a rather sharp cutoff. This behaviour is surprising for the following reasons. If generation of, for example, the 25th harmonic becomes as probable as fifth-order harmonic generation, as is the case for a Nd-YAG laser at an intensity of $3 \times 10^{13}$ W cm$^{-2}$ in a 10 Torr argon vapour (Li *et al* 1989), it means that the weak-field picture (see e.g. Gontier and Trahin 1982, Gao and Starace 1989, Potvliege and Shakeshaft 1989a, Pan *et al* 1989, 1990), which has been successfully applied for describing (non-resonant) non-linear optical phenomena before, does not apply anymore. One has to go beyond lowest-order perturbation theory for providing a correct description of these non-linear optical phenomena where the field is no longer a weak perturbation of the atomic medium. Time-dependent approaches involving the numerical solution of the Schrödinger equation (Kulander and Shore 1989, 1990, DeVries 1990, LaGattuta 1990) and Floquet calculations (Potvliege and Shakeshaft 1989b) have been successfully employed. Classical methods (Bandarage *et al* 1990, Chu *et al* 1990), one-dimensional approximations (Eberly *et al* 1989a, b, c) and many other model calculations (Shore and Knight 1987, Biedenharn *et al* 1989, Becker *et al* 1990, Sundaram and Milonni 1990) also provide some insight into the physics involved. The single-atom photoemission spectra from all these calculations generally reproduce qualitatively the experimental data. This is another interesting and surprising aspect of the problem. Phase-matching conditions are known to play an important role in the overall response of the medium and to be very sensitive to various parameters such as the atomic density, the focusing geometry, the laser frequency and the process order. On the basis of weak-field calculations of harmonic generation, one would expect phase matching to severely degrade with the order (Shore and Kulander 1989, L'Huillier *et al* 1990). In contrast, the comparison between experimental data and single-atom calculations seems to indicate that propagation effects either play no role or affect all the harmonics in the same way.

Thus, the interpretation of the experimental results is not an easy task because it involves both the single-atom response to a strong laser interaction and the many-atom response, the capability of the medium to ensure proper phase matching between the (non-perturbative) non-linear polarization induced by the incident field and the propagating harmonic radiation. The purpose of the present paper is to discuss this double aspect (microscopic and macroscopic) of harmonic generation processes. The conversion efficiency depends both on the quantities which govern the interaction of a laser with a single atom, the atomic system, the laser wavelength and intensity, and also on the parameters which affect the propagation of the fields such as the atomic density or the interaction geometry. Our emphasis will be on this latter part (propagation), which has received little attention up to now, whereas in contrast, a lot has been done concerning harmonic generation by a single atom (see the references mentioned above).

Studies of harmonic generation in gases up to 1987 have been extremely well documented in reviews and textbooks (Hanna *et al* 1979, Reintjes 1984, Shen 1984, Arkhipkin and Popov 1987, Delone and Krainov 1988). The experimental and theoretical results obtained more recently have been described by L'Huillier *et al* (1991b) and we refer the reader to this work for a comprehensive review. In the present paper, we chose to focus our attention on fewer results which we analyse as thoroughly as possible. We present the theoretical method used for describing these harmonic conversion processes. It consists first in the calculation of the single-atom photoemission spectrum performed by numerically integrating a time-dependent Schrödinger equation (Kulander and Shore 1989, 1990). Then, we solve the paraxial propagation equation using as a source the non-linear polarization induced by the radiating atomic dipoles.

Our method is applied to the interpretation of one particular result, harmonic generation in a 15 Torr xenon vapour irradiated by a 1064 nm Nd–YAG laser at intensities of the order of $10^{13}$ W cm$^{-2}$ (L'Huillier *et al* 1991c).

The paper is organized as follows. In section 2, we present in parallel experimental results and the single-atom calculations. Although the emphasis of this paper is essentially theoretical, we thought it useful to include a summary of the experimental method and of the main results. We describe in particular the results obtained in xenon (Li *et al* 1989, Lompré *et al* 1990) which provide the basis for our theoretical analysis. We present the corresponding single-atom emission spectra. This is the first part of our theoretical analysis, which will allow us to separate the contribution of the single-atom response and that of phase matching, an essential step in the understanding of the experimental results. We also give some details about the method used for integrating the time-dependent Schrödinger equation (Kulander and Shore 1989, 1990). In section 3, we develop a formalism for describing the generation and propagation of harmonics in a medium exposed to a strong laser field. We show how this can be applied to the analysis of the experiments performed in xenon at 1064 nm. Our final results agree well with the experimental observations, reproducing in particular the plateau behaviour. We try to unravel the role of phase matching in strong-field harmonic generation.

## 2. Experimental results and single atom photoemission spectra

### 2.1. Experimental studies

*2.1.1. Method.* A harmonic generation experiment consists of focusing an intense laser radiation into a rather dense rare-gas medium (a few Torr) and then analysing along the propagation axis the VUV light emitted during the interaction. A schematic picture of the experiment principle is shown in figure 1. Most of the experiments reported here have been done by using a mode-locked Nd–YAG laser (40 ps pulse width, 1064 nm wavelength), with a maximum energy of 1 GW at a 10 Hz repetition rate. The linearly polarized laser is focused into the interaction chamber. A useful quantity
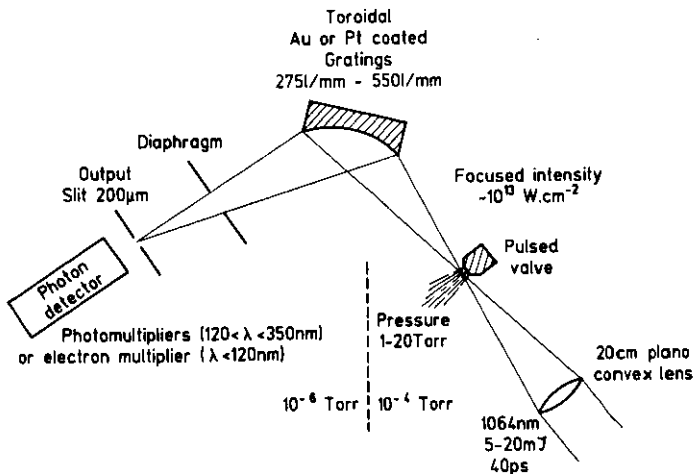


**Figure 1.** Experimental set-up for the detection of VUV light employed in Saclay.

which characterizes the focus is the confocal parameter $b = 2\pi\omega_0^2/\lambda$, $\omega_0$ denoting the beam radius and $\lambda$ the wavelength. For a Gaussian beam, $b$ is equal to twice the distance on the propagation axis over which the beam section increases by a factor of two.

A pulsed gas jet (Kung 1983, Bokor *et al* 1983) produces a well collimated atomic beam with a 15 Torr pressure at 0.5 mm below the nozzle of the jet (Lompré *et al* 1988). The atomic density distribution in the jet has been measured to be very close to a Lorentzian distribution with a 1 mm full width at half maximum ($L$). An advantage of gas jets compared with differential pumping systems is that low background pressures can be kept in the interaction chamber and in the detection chamber (see figure 1) with reasonable pumping equipment. Moreover, the interaction region is small (typically 1 mm long) and it can be exposed to an intense laser pulse in an almost collimated beam geometry. This can be very advantageous for phase matching in a positively dispersive medium (L'Huillier *et al* 1988) and for avoiding significant absorption of the emitted radiation.

The VUV detection system, which covers a broad spectral range from 10 to 350 nm, is described in figure 1. A grazing incidence holographic grating separates the different components of the light emitted along the propagation axis. The light is then detected by photomultipliers ($\lambda > 120$ nm) or electron multipliers ($\lambda < 120$ nm). This monochromator has a good detection efficiency owing to the lack of an entrance slit (see figure 1). The number of photons produced at each frequency can be estimated to within one order of magnitude by using the spectral efficiency of the photon converter, the grating efficiency and the absolute electron multiplier gain.

*2.1.2. Results.* Typical spectra consist of series of harmonic peaks superposed on a broad background. Figure 2 shows, for example, the spectrum between 70 nm and 110 nm obtained in Xe at 1064 nm, $3 \times 10^{13}$ W cm$^{-2}$ with a 75 mm focal lens. Although the monochromator did not have a sufficient resolution for separating all the lines, most of the features could be attributed to discrete transitions in Xe, Xe$^+$, Xe$^{2+}$. This fluorescence background is probably due to dielectronic recombination processes, following the formation of a plasma by multiphoton ionization. These processes occur on a much longer time scale than harmonic generation and at an intensity high enough for ionizing—at least partially—the non-linear medium. This light emission is incoherent and probably isotropic. Whether there is an underlying continuous background is
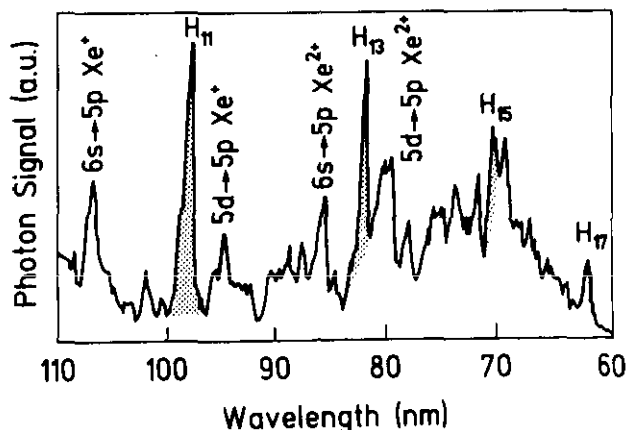


**Figure 2.** Xe spectrum obtained at 1064 nm, $3 \times 10^{13}$ W cm$^{-2}$.

an open question: these processes should be studied with better resolution and at another detection angle (e.g. perpendicularly to the laser axis).

In figure 3, the number of photons produced in a 15 Torr xenon vapour is plotted as a function of the harmonic order for several laser intensities between $5 \times 10^{12}$ W cm$^{-2}$ and $3 \times 10^{13}$ W cm$^{-2}$ (Lompré *et al* 1990). This result has been obtained with a 200 mm focal length (the confocal parameter $b$ is estimated to be 4 mm). Only *odd* harmonics are observed, which is to be expected for harmonic generation in an isotropic gaseous medium, with inversion symmetry. At the lowest intensity ($5 \times 10^{12}$ W cm$^{-2}$), the harmonic signal decreases with the order. As the intensity increases, a plateau followed by a rather abrupt cutoff appears. Its length increases with the laser power, up to the intensity at which the medium becomes ionized with a probability close to unity, above $1.3 \times 10^{13}$ W cm$^{-2}$. Above this intensity, the signal increases much less rapidly, the distribution becomes smoother but the maximum observable harmonic order remains constant (equal to 21 for this pulse length). The vertical scale gives an order of magnitude estimate of the number of photons produced at each laser shot. This means a power efficiency of $10^{-8}$–$10^{-9}$ for the plateau harmonics at the highest laser intensity. The brightness is estimated to be $10^{17}$ photons/s Å mrad$^2$.

Another way of looking at these results is to plot the number of photons as a function of the laser intensity. Figure 4 shows, for example, the behaviour of the 15th harmonic. All the intensity dependences of the harmonics present a common feature: the number of photons increases first rapidly, then saturates when the medium gets ionized. There are two reasons why the ionization of the gas limits harmonic generation (Miyazaki and Kashiwagi 1978, Reintjes 1984, L'Huillier *et al* 1990). The main medium responsible for harmonic generation (the neutral atoms) gets depleted when the medium becomes ionized. Harmonics are still produced in the periphery of the interaction volume or at the beginning of the laser pulse. Ions could also generate harmonics, but their response is expected to be less efficient at these intensities. The second effect that might limit harmonic conversion efficiencies is the breaking of phase matching owing to the presence of free electrons in the medium. These free electrons have a non-negligible effect on the refractive index (at the fundamental frequency and at the
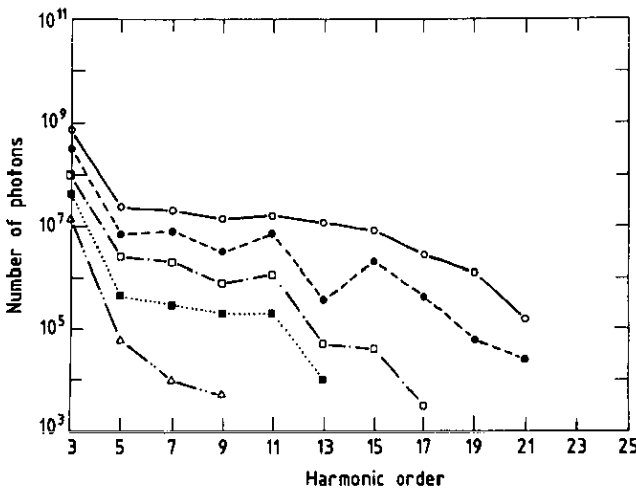


**Figure 3.** Number of photons produced in xenon at 1064 nm as a function of the harmonic order. The intensities are, from top to bottom, $3 \times 10^{13}$ W cm$^{-2}$ (—○—), $1.3 \times 10^{13}$ W cm$^{-2}$ (——●——), $9 \times 10^{12}$ W cm$^{-2}$ (—·—□—·—), $7 \times 10^{12}$ W cm$^{-2}$ (···■···), $5 \times 10^{12}$ W cm$^{-2}$ (··—△—··).
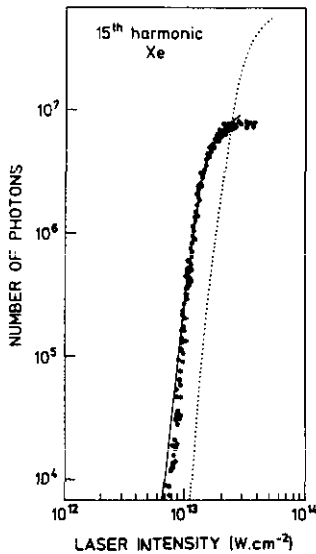
**Figure 4.** Fifteenth harmonic in Xe as a function of the laser intensity in a double logarithmic plot. The full circles are the experimental results. The dotted curve shows the result of our calculation (see section 3.3). The full curve has been obtained by shifting the intensity scale so that the calculated and experimental saturation intensities agree and by scaling the calculated harmonic signals.

harmonic frequencies). They induce a large positive phase mismatch between the generated beam and its driving polarization, which can reduce the conversion efficiency (see section 3.3).

Below saturation, the harmonics vary as some power law of the laser intensity (Lompré *et al* 1990). The lowest order harmonics ($q \leqslant 9$) vary as predicted by lowest order perturbation theory. The 11th and 13th harmonics exhibit a more complex intensity dependence, which might be due to the influence of discrete resonances and which is much less rapid than the $I^{11}$ or $I^{13}$ perturbative power laws. The highest harmonics vary all in the same way, approximately as the 12th power of the laser intensity. This is consistent with the plateau observed in the harmonic intensity distributions (figure 3). Indeed, the fact that there is a plateau means that all the harmonics must have approximately the same power law. Because the intensity dependences deviate from a $I^q$ power law, where $I$ is the laser intensity and $q$ the process order, the atomic response cannot be described within the weak-field limit. The measured power law reflects, however, both the single-atom contribution and the collective response of medium (phase matching) which may also be power dependent.

Similar results have been obtained with the other heavy rare gases (krypton and argon). The distributions obtained in Xe, Kr, Ar at $3 \times 10^{13}$ W cm$^{-2}$ are shown in figure 5 (Li *et al* 1989). The conversion efficiency decreases from Xe to Ar, which is not surprising, since xenon is more polarizable than lighter rare gases. However, the maximum order that can be observed increases from 21 in Xe, 29 in Kr to 33 in Ar. The 33rd harmonic (32 nm, 38 eV) is the shortest wavelength radiation produced with the Nd–YAG laser system (limited, however, to about 20 mJ in 40 ps). Atoms with higher ionization energies have in general a lower conversion efficiency but they can produce more harmonics. Moreover, they can experience a higher laser intensity without being ionized.
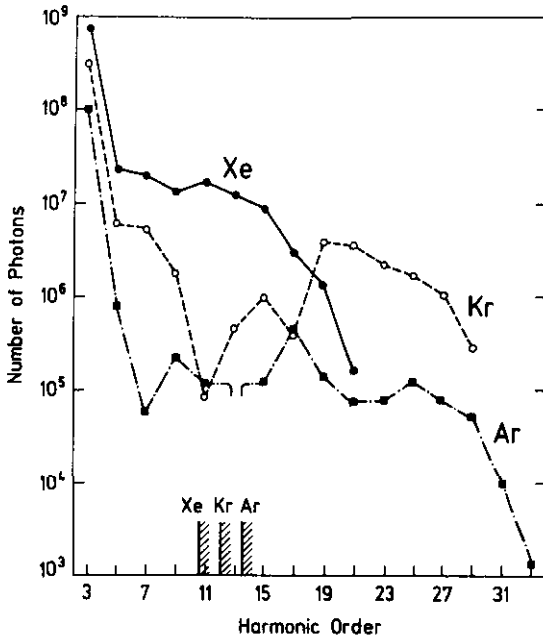
**Figure 5.** Number of photons produced in Xe, Kr, Ar at $3 \times 10^{13}$ W cm$^{-2}$, 1064 nm.

Shortening the laser pulse length also increases the intensity at which an atom ionizes and therefore might lead to the production of higher order harmonics. Recently, the 53rd harmonic of a 1 ps, 1 $\mu$m Nd–glass laser was reported in neon at an intensity of $5 \times 10^{14}$ W cm$^{-2}$ (L'Huillier *et al* 1991a).

Other experimental studies involve the variation of the parameters that influence the macroscopic aspect of the interaction, the atomic density and the focusing conditions. Let us briefly summarize the main conclusions. First, the harmonic signal is found to vary as the square power of the atomic pressure (from 1 to 25 Torr) independent of the gas, the harmonic order and the laser intensity (Li *et al* 1989). This is the signature of a coherent process. Indeed, an incoherent sum of single-atom dipole radiation would give a linear dependence of the signal on the atomic density. The square dependence shows that the measured light results from a *coherent* sum of the radiating dipoles. (In the first case, one sums the intensities; in the second case, one sums the amplitudes and then squares.)

The second study is of the dependence of the signal on the interaction geometry (i.e. on the volume within which the harmonics are created). This helps in understanding phase matching, which is expected to be strongly affected by focusing (Bjorklund 1975, L'Huillier *et al* 1990). As will be shown in section 3, the measured number of photons is proportional to $b^3 |F_q(b)|^2$, where $b$ is the confocal parameter, proportional to the focal section $S$ and where the quantity denoted $|F_q(b)|^2$, the square of the phase matching function, reflects the propagation of the fields throughout the medium. The $b^3$ factor has the following origin: $b^2$ arises from the coherence of the process, the fact that the harmonic signal varies as the square of the number of atoms involved. Since the medium is limited in the propagation direction by the length of the gas jet, this must be understood as the number of atoms in the transverse direction, in the focal plane, so that the number of photons then varies as $S^2$ or $b^2$. The detected signal is a

number of photons, proportional to the focal section of the harmonic field, which is itself proportional to the focal section of the incident field $S$. Hence the additional factor of $b$. Experiments have been performed with different geometries (Lompré *et al* 1990) varying from confocal focusing ($b \approx L$) to a plane-wave situation ($b \gg L$). In figure 6, we compare the harmonic intensity distributions obtained with $b = 1$, 4 and 6 mm and $L = 1$ mm at a $1.3 \times 10^{13}$ W cm$^{-2}$ laser intensity. The signal has been divided by the global factor $b^3$. The difference between the three results, which then reflects the variation of the phase matching factor $|F_q(b)|^2$ with $b$, lies within the experimental error bar. With $b = 1$ mm, harmonics higher than the 15th could not be detected. That is simply due to a harmonic/background ratio which was barely above one in this case. This result shows that phase matching ($|F_q(b)|^2$) does not depend much on the focusing geometry. This contradicts predictions derived from the weak-field limit (L'Huillier *et al* 1990; see section 3) and emphasizes the need for a general, non-perturbative, description of harmonic generation processes. Another important practical conclusion is that using a loosely focused geometry considerably enhances the conversion efficiency (as $b^3$).
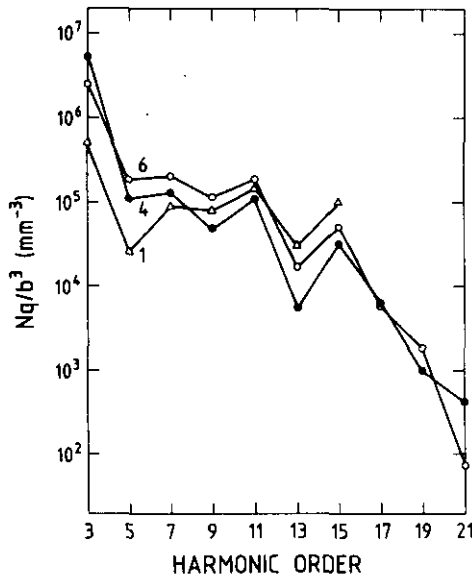


**Figure 6.** Number of harmonic photons divided by $b^3$ in Xe at $1.3 \times 10^{13}$ W cm$^{-2}$. $\triangle$, $b = 1$ mm; $\bullet$, $b = 4$ mm; $\bigcirc$, $b = 6$ mm (Lompré *et al* 1990).

## 2.2. Harmonic generation by a single atom

The electrons in an atom oscillate in response to a strong laser field. This acceleration of the charge density causes the emission of radiation at odd multiples of the driving frequency. If the field is not too strong, the rate of emission can be calculated using standard perturbative methods. Following the pioneering work of Manakov *et al* (1975), Manakov and Ovsyannikov (1980) and Gontier and Trahin (1982), very accurate high-order non-linear susceptibilities have been obtained by Potvliege and Shakeshaft (1989a), Pan *et al* (1989, 1990) and Gao and Starace (1989) for hydrogenic systems.

The calculations of perturbative emission rates for multielectron systems are substantially more difficult, with only the lower order susceptibilities of some of the rare gases having been reported (see e.g. Sitz and Yaris 1968, Manakov *et al* 1975, Manakov and Ovsyannikov 1980, Bishop *et al* 1988).

The strong-field emission from atomic systems has been successfully investigated using two different approaches. First, the expansion of the electronic wavefunction in a Floquet basis has been used by Potvliege and Shakeshaft (1989b) to obtain nonperturbative harmonic emission rates by hydrogen for driving frequencies of 1064 and 532 nm. This method is valid for intensities up to the point where the ionization rate becomes comparable with the laser frequency. For intensities beyond this regime, the assumption of a constant intensity pump is invalid and the atomic response becomes very sensitive to the pulse shape.

The second approach for modelling photoemission from laser excited atoms is the direct solution of the time-dependent Schrödinger equation. This has been accomplished for a number of one-dimensional model systems by Eberly *et al* (1989a, b, c) and by Sacks and Szöke (1991); for several model systems by Becker *et al* (1990) and Sundaram and Milonni (1990); for a classical electron in the field of a proton by Bandarage *et al* (1990), Chu *et al* (1990) and for realistic, three-dimensional atoms by Kulander and Shore (1989, 1990), DeVries (1990) and LaGattuta (1990).

*2.2.1. Method.* We briefly present the details of the single-electron atomic calculations. The time-dependent Schrödinger equation for a hydrogen atom in a linearly polarized field, using the length gauge, is

$$\mathrm{i}\frac{\partial}{\partial t}\Psi(\mathbf{r},t) = \left(-\tfrac{1}{2}\nabla^2 - \frac{1}{r} - E_0 f(t) z \sin(\omega t)\right)\Psi(\mathbf{r},t) \tag{2.1}$$

where $E_0$ is the peak amplitude of the field and $f(t)$ is the pulse envelope. We use a mixed basis representation, first expanding the wavefunction in spherical harmonics

$$\Psi(\mathbf{r},t) = \sum_{l=0}^{L} \phi_l(r,t) Y_{l0}(\hat{r}) \tag{2.2}$$

and then discretizing along the radial axis

$$\phi_l(r,t) \to \phi_l(r_j,t) \to \phi_l^j \tag{2.3}$$

with $r_j = (j-0.5)\Delta r$. $L$ is adjusted as required to achieve convergence. Using a three-point formula for the second derivative, and defining $g_l^j = r_j \phi_l^j$, we can rewrite (2.1) as

$$\mathrm{i}\frac{\partial}{\partial t} g_l^j = (H_0 g)_l^j + (H_1 g)_l^j \tag{2.4}$$

where $H_0$, the atomic Hamiltonian, couples radial values $j$ to $j, j\pm 1$ and is diagonal in $l$, while $H_1$, the interaction term, couples angular momenta $l$ to $l\pm 1$ and is diagonal on $j$. In treating many-electrons atoms, we have used effective potentials (Kulander and Rescigno 1991) which are $l$-dependent functions of the radial coordinate. The potentials are based on Hartree–Slater calculations for the ground and lower excited states of the atom. The time-dependent calculations for these systems treat the excitation of a single electron in the presence of the other electrons which are frozen in their ground-state orbitals. Thus we have neglected excitation pathways which involve double or multiply excited states. This choice of potential does not alter the tridiagonal forms of $H_0$ and $H_1$.

The time propagation is carried out using the Peaceman–Rachford alternating directions implicit scheme (Varga 1962),

$$g_i^j(t+\Delta t) = [I+iH_0\tau]^{-1}[I+iH_1\tau]^{-1}[I-iH_1\tau][I-iH_0\tau]g_i^j(t) \qquad (2.5)$$

where I is the unit matrix and $\tau = \Delta t/2$. The interaction term is evaluated at the midpoint of the time step. Since the matrices in the brackets are all tridiagonal, the multiplication and inversion can be achieved with vector operations. The propagator is accurate to second order in the time step and is approximately unitary. The computational effort in solving (2.4) is linear in the number of grid points. We can propagate more than $1.2 \times 10^6$ spacetime points per second on a Cray Y/MP machine.

The prompt emission by an atom in an intense field is due to the oscillation of the electron charge density in the vicinity of the nucleus. Electrons at large radial distances cannot emit high energy photons because momentum cannot be conserved. Therefore, we determine the time-dependent wavefunction in a limited volume near the nucleus by removing the flux which reaches the edges of our grid with a mask function which forces the amplitude smoothly to zero at the boundary. This mask function is applied after each integration step.

The calculation proceeds as follows. We choose a pulse shape, $f(t)$ in (2.1), which rises as the square of a sine function over five optical cycles, then is unity for the next 15–30 cycles. During the first part of the constant intensity interval the transient excitations which occurred during the ramp decay by ionization. Then during the latter part of this interval, we determine the photoemission spectrum and rates. These we obtain by Fourier transforming the time-dependent induced dipole,

$$d(\omega) = \frac{1}{T_1 - T_2} \int_{T_1}^{T_2} dt \, e^{-i\omega t} \langle \Psi(r,t)|z|\Psi(r,t)\rangle \qquad (2.6)$$

over the last five cycles of the pulse.

*2.2.2. Results.* In figure 7 we show a complete emission spectrum for xenon in a 1064 nm laser at an intensity of $3 \times 10^{13}$ W cm$^{-2}$. The spectrum displays narrow peaks
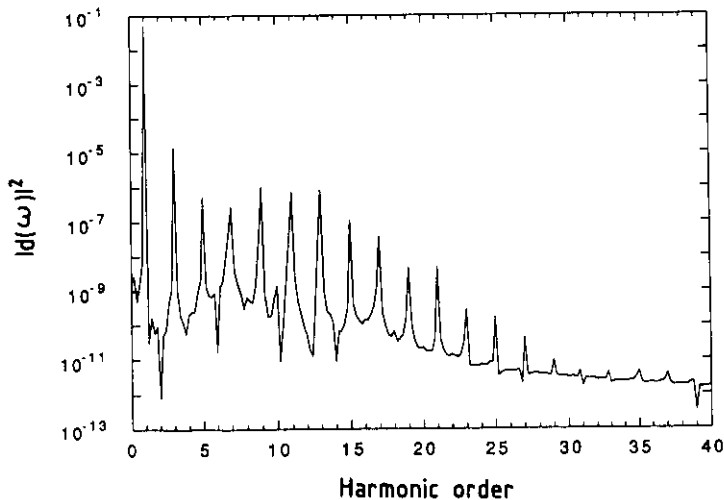
**Figure 7.** Xenon spectrum at $3 \times 10^{13}$ W cm$^{-2}$, 1064 nm, obtained from the time-dependent integration of the Schrödinger equation.

at odd multiples of the driving frequency above a broad background. The width of the harmonic peaks is determined by the lesser of the two intrinsic time scales in the problem, the ionization time or the pulse length. The background is quite sensitive to the integration parameters (Krause *et al* 1991) and has no constant phase relationship to the driving field. Therefore, no phase matched, coherent background signal can be expected. The harmonics do have a well defined but intensity-dependent phase delay which weakly affects the phase matching of these fields.

We have performed calculations for a fine grid of intensities between $5 \times 10^{12}$ and $5 \times 10^{13}$ W cm$^{-2}$. In figure 8, the harmonic emission strengths for several of these intensities are displayed. This figure shows the emergence of a plateau which increases in strength and extent with increasing pump intensity. The harmonics initially rise very quickly with intensity as predicted by perturbation theory, then rise substantially more slowly with numerous oscillations due to intermediate resonance effects. The intensity dependences of the 3rd, 9th, 17th and 23rd harmonics are shown in figure 9. Only the third harmonic behaves approximately as $I^3$ over this intensity range. The approximate power laws for the higher harmonics are much lower than their orders, being approximately $I^6$ for those in the plateau. They are also lower than the experimental power laws.
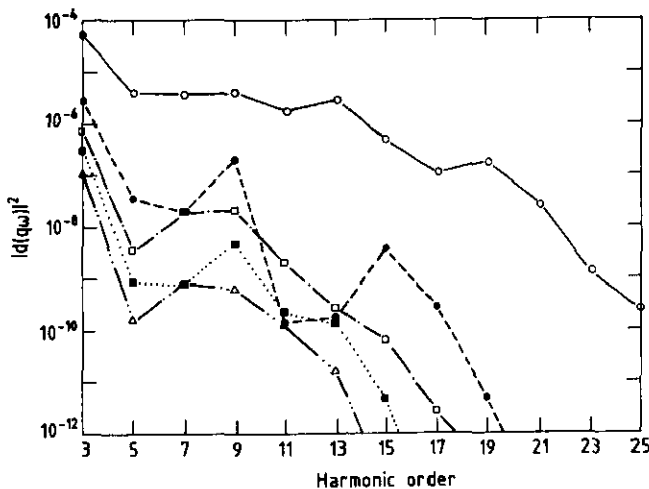


**Figure 8.** Intensity of the dipole moment $|d(q\omega)|^2$ (au) as a function of the harmonic order $q$, at the same laser intensities as in figure 3.

Similar studies of other rare-gas atoms qualitatively reproduce the observed trends in the harmonic conversion efficiencies. The highest conversion efficiency, for a given pump intensity, was found in xenon which is the most polarizable of the atoms studied. The broadest plateau in the spectrum was found in the system with the highest ionization potential. In figure 10 we show a comparison of the single-atom spectra for Ar, Kr and Xe at $3 \times 10^{13}$ W cm$^{-2}$. Allowing for the difference in ionization rates for these three atoms, the shapes of the harmonic spectra in the figure agree very well with the measurements shown in figure 5 (Li *et al* 1989). In order to compare the yields directly, however, the effects of phase matching during the propagation of the harmonic fields through the medium must be determined.
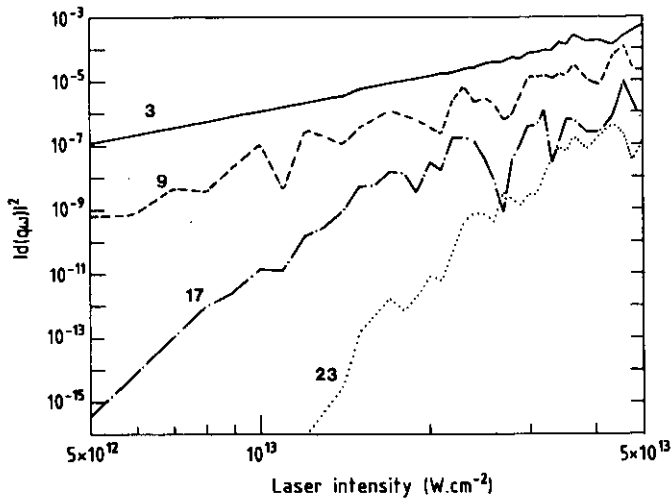
**Figure 9.** Intensity dependences of the 3rd, 9th, 17th and 23rd harmonic components of the dipole moment in xenon (atomic units).
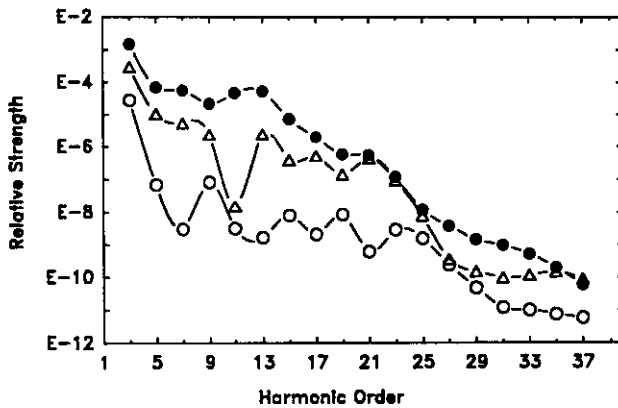


**Figure 10.** Comparison between the harmonic spectra of Xe ($-\bullet-$), Kr ($-\triangle-$), Ar ($-\bigcirc-$) at $3 \times 10^{13}$ W cm$^{-2}$ and 1064 nm (Kulander and Rescigno 1991).

## 3. Harmonic generation by an assembly of atoms exposed to an intense field

We first give a general theoretical framework for the description of harmonic generation in a gaseous medium. Then, we analyse the phase matching conditions for the experiments reported in section 2.1 within the weak-field limit, using traditional non-linear optics arguments. In section 3.3, we give the results of a more complete calculation for the propagation of the harmonic fields, which uses as a source the response of an atom exposed to a strong field (see section 2.2). These two calculations lead to opposite conclusions. We find that phase matching of the high harmonics is considerably enhanced in a strong-field regime as compared with the weak-field limit. As will be explained in section 3.4, this is mainly an *amplitude* effect, related to the harmonics power law, which is much lower in a strong-field situation than in the perturbative case.

## 3.1. Theoretical framework

We start from the general wave equation describing the propagation of an electromagnetic field $\mathscr{E}(r, t)$ in an isotropic dielectric medium characterized by an electronic polarization $\mathscr{P}(r, t)$.

$$\nabla^2 \mathscr{E} - \frac{1}{c^2} \frac{\partial^2 \mathscr{E}}{\partial t^2} = \frac{4\pi}{c^2} \frac{\partial^2 \mathscr{P}}{\partial t^2}. \tag{3.1}$$

When the incident field is linearly polarized, this is a scalar equation, in the direction of the laser field. $\mathscr{E}(r, t)$ and $\mathscr{P}(r, t)$ can be expanded as

$$\mathscr{E}(r, t) = \tfrac{1}{2}\left(\sum_q \mathscr{E}_q(r, t) \, e^{-iq\omega t} + \mathrm{CC}\right) \qquad \mathscr{P}(r, t) = \tfrac{1}{2}\left(\sum_q \mathscr{P}_q(r, t) \, e^{-iq\omega t} + \mathrm{CC}\right). \tag{3.2}$$

The Fourier transform of (3.1) gives a set of coupled equations

$$\nabla^2 \mathscr{E}_q + \left(\frac{q\omega}{c}\right)^2 \mathscr{E}_q = -4\pi \left(\frac{q\omega}{c}\right)^2 \mathscr{P}_q. \tag{3.3}$$

The polarization of the medium is the distribution of dipole moments induced by the total electric field (and not simply by the laser field). It is the sum of the linear polarization $\mathscr{P}_q^L = \mathcal{N}\chi^1(-q\omega; q\omega) \, \mathscr{E}_q$ where $\chi^1(-q\omega; q\omega)$ is the field-free dipole polarizability and the non-linear polarization $\mathscr{P}_q^{NL}$, which itself contains a number of terms involving the fundamental and the harmonic fields. Among those terms, we can distinguish the non-linear polarization induced by the fundamental field, which is the driving term for harmonic generation, denoted by $\mathscr{P}_q^d$. There are higher order terms to the linear polarization at frequency $q\omega$, which lead to intensity-dependent corrections to the refractive index (Zych and Young 1978, Mahon and Yiu 1980, Ganeev *et al* 1985, Drabovich *et al* 1985, Malcuit *et al* 1990). Finally, the non-linear polarization also includes all kinds of wave-mixing processes involving several harmonic fields (Tomov and Richardson 1976, Groseva *et al* 1977, Reintjes 1984). For example, the fifth harmonic can be created from the interaction of the third harmonic field and the fundamental (absorption of one photon at frequency $3\omega$, plus absorption of two photons at frequency $\omega$). The ninth harmonic can be created from third harmonic generation of the third harmonic field, or from the seventh harmonic, plus absorption of two laser photons, etc. The number of possible mixing processes increases very rapidly with the order. In the high-order harmonic generation experiments in gaseous media discussed in the present paper, however, the harmonic conversion efficiency remains weak, so that these indirect processes can be neglected. The study of the pressure dependence of the harmonic signal also indicates that such processes which would exhibit a much higher pressure dependence than $\mathcal{N}^2$ cannot be very important. In the same way, we neglect depletion of the pump field, which has to be taken into account for high conversion efficiencies (Tomov and Richardson 1976, Puell *et al* 1976, Kildal and Brueck 1980). These approximations allow us to decouple the equations describing propagation of the harmonics. Introducing the intensity-dependent dipole polarizability $\chi^1(q\omega, |\mathscr{E}_1|^2)$, (3.3) can be written as

$$\nabla^2 \mathscr{E}_1 + (\omega/c)^2[1 + 4\pi\mathcal{N}\chi^1(\omega, |\mathscr{E}_1|^2)]\mathscr{E}_1 = 0 \tag{3.4}$$

for the fundamental, and

$$\nabla^2 \mathscr{E}_q + (q\omega/c)^2[1 + 4\pi\mathcal{N}\chi^1(q\omega, |\mathscr{E}_1|^2)]\mathscr{E}_q = -4\pi(q\omega/c)^2 \mathscr{P}_q^d \tag{3.5}$$

for the harmonic fields.

Equation (3.4) describes the propagation of an intense laser beam in a medium, including non-linear effects such as self-focusing (Grishkowsky 1970, Akhmanov *et al* 1972, Marburger 1975, Shen 1984). We neglect these effects, which are weak for long incident wavelengths and at relatively low atomic densities, as well as the (defocusing) effects which may arise from the presence of free electrons. $\mathscr{E}_1$ is then simply the laser field propagating into a medium characterized by the refractive index $n_1$ (wavevector $k_1 = \omega/c(1 + 2\pi\mathcal{N}\chi^1(-\omega, \omega)) = n_1\omega/c)$.

Equation (3.5) describes harmonic generation in a medium exposed to a strong laser field, for weak harmonic conversion efficiencies. However, its solution with non-perturbative polarizations and refractive indices remains a formidable problem, and we shall make an additional approximation which will allow us to use a simple procedure for solving numerically the propagation equation. We shall neglect higher-order corrections to the refractive index at frequency $q\omega$ as we do for the fundamental, though it may not be justified for harmonic frequencies close to the ionization threshold (in the resonance region) and above. However, as will be shown below, the effect of dispersion (i.e. the fact that the refractive index varies with the wavelength, whether it is intensity dependent or not) remains small in the experiments performed at Saclay, at a relatively low pressure. Equation (3.5) then becomes

$$\nabla^2\mathscr{E}_q + k_q^2\mathscr{E}_q = -4\pi(q\omega/c)^2\mathscr{P}_q^d. \tag{3.6}$$

The homogeneous part of this differential equation is linear and we can therefore use an integral representation (Kleinman 1962, Bloembergen 1965, Lago *et al* 1987). The outgoing Green function associated with the homogeneous part of (3.6) is $e^{ik_qR}/4\pi R$, with $R = |r - r'|$. (3.6) can be written as (Jackson 1975)

$$\mathscr{E}_q(r') = \left(\frac{q\omega}{c}\right)^2 \int \frac{e^{ik_qR}}{R}\mathscr{P}_q(r)\,d^3r. \tag{3.7}$$

(From now on, we drop the d index in $\mathscr{P}_q^d$.) We assume that the field is emitted close to the propagation axis (paraxial approximation). We are interested in the harmonic field outside the medium, in the *far field*. Let $r = (x, y, z)$ be a point in the medium and $r' = (x', y', z')$ the observation point, far from the sources. The far-field approximation implies that $|z' - z| \gg |x' - x|$, $|y' - y|$ so that $R \approx z' - z + [(x' - x)^2 + (y' - y)^2]/2(z' - z)$. Equation (3.7) becomes

$$\mathscr{E}_q(r') = \left(\frac{q\omega}{c}\right)^2 \int \frac{\mathscr{P}_q(r)}{z' - z} \exp[ik_q(z' - z)] \exp\left(\frac{ik_q[(x' - x)^2 + (y' - y)^2]}{2(z' - z)}\right) d^3r. \tag{3.8}$$

Finally, introducing the slowly varying envelopes $E_q = \mathscr{E}_q \exp(-ik_qz)$ and $P_q = \mathscr{P}_q \exp(-iqk_1z)$, the harmonic profile in the far field takes the simple form:

$$E_q(r') = \left(\frac{q\omega}{c}\right)^2 \int \frac{P_q(r)\,e^{-i\Delta k_qz}}{z' - z} \exp\left(\frac{ik_q[(x' - x)^2 + (y' - y)^2]}{2(z' - z)}\right) d^3r \tag{3.9}$$

where $\Delta k_q = k_q - qk_1$ is the phase mismatch between the polarization field and the harmonic field ($\Delta k_q \ll k_q$, $qk_1$). Absorption and ($z$-dependent) atomic density distributions (Rettner *et al* 1984, Lago *et al* 1987) can be accounted for simply by replacing $\Delta k_q z$ in the exponential in (3.9) by the expression

$$\{\Delta kz\} = \int_{-\infty}^{z} \Delta k_q(z'')\,dz'' - i\int_{-\infty}^{+\infty} \kappa_q(z'')\,dz'' \tag{3.10}$$

where $\kappa_q(z) = \text{Im}(\Delta k_q(z))$ is the absorption coefficient at frequency $q\omega$, equal to $\mathcal{N}(z)\sigma_q/2$, where $\sigma_q$ is the photoionization cross section and $\mathcal{N}(z)$ the atomic density distribution.

The solution of the propagation equation thus reduces to a straightforward three-dimensional integral over the non-linear medium. The last problem that needs to be understood in order to calculate propagation of the harmonics, particularly in a strong-field situation, is how to relate the Fourier components $d_q$ ($= d(q\omega)$ of (2.6)) of the dipole moment $d(t)$ calculated for a real field $\mathscr{E}(t) = \mathscr{E} \cos \omega t$, to the propagating non-linear polarization $\mathscr{P}_q = P_q(r) e^{iqk_1z}$ resulting from the interaction of a focused beam with the medium. Consider, for example, an incident Gaussian beam (this is what we shall use in our calculation, though this argument is much more general).

$$E_1(r, z) = \frac{bE_0}{b + 2iz} \exp\left(-\frac{k_1 r^2}{b + 2iz}\right). \tag{3.11}$$

The real part of a Gaussian beam $E_1(r, z) e^{i(k_1 z - \omega t)}$ can be written as $|E_1(r, z)| \cos[\omega t + \varphi(r, z)]$, with

$$|E_1(r, z)| = \frac{bE_0}{(b^2 + 4z^2)^{1/2}} \exp\left(-\frac{k_1 r^2 b}{b^2 + 4z^2}\right) \tag{3.12}$$

and

$$\varphi(r, z) = -k_1 z + \tan^{-1}(2z/b) - \frac{2k_1 r^2 z}{b^2 + 4z^2}. \tag{3.13}$$

The polarization $P_q(r, z)$ can therefore be obtained from the time-dependent dipole moment calculated for a field strength $|E_1(r, z)|$ and evaluated at a time $t' = t + \varphi(r, z)/\omega$. The expression for the envelope $P_q(r, z)$ is then

$$P_q(r, z) = 2\mathcal{N}(z)d_q(r, z) \exp\left[-iq\left(\tan^{-1}(2z/b) - \frac{2k_1 r^2 z}{b^2 + 4z^2}\right)\right] \tag{3.14}$$

where $d_q(r, z)$ denotes the $q$th harmonic component of the time-dependent dipole moment evaluated for a field strength $|E_1(r, z)|$. In the weak-field limit, $d_q(r, z)$ is related to the $q$th-order non-linear susceptibility $\chi^q$ (Reintjes 1984) by

$$d_q(r, z) = \mathcal{N}(z) \frac{\chi^q}{2^q} |E_1(r, z)|^q. \tag{3.15}$$

In this case, the integral in (3.9) can be performed almost completely analytically. In a more general situation, where $d_q(r, z)$ cannot be expressed simply as a function of the incident field, (3.9) needs to be performed numerically. Note that by making use of the revolution symmetry of the problem, it actually reduces to a two-dimensional integral

$$E_q(r', z') = \left(\frac{q\omega}{c}\right)^2 \int \frac{P_q(r, z) \exp(-i\{\Delta k z\})}{z' - z}$$

$$\times \exp\left(\frac{ik_q(r^2 + r'^2)}{2(z' - z)}\right) J_0\left(\frac{k_q r r'}{z' - z}\right) 2\pi r \, dr \, dz \tag{3.16}$$

where $J_0$ denotes the zero-order Bessel function. To conclude this section, we give the expression for the total number of photons emitted, $N_q$, which is the quantity measured

experimentally. Assuming that the laser pulse width is long compared with the light period, $N_q$ is obtained by integrating the harmonic intensity profile both spatially and temporally

$$N_q = \frac{c}{4\hbar q\omega} \int r'|E_q(r', z', t')|^2 \, \mathrm{d}r' \, \mathrm{d}t'. \tag{3.17}$$

### 3.2. Phase matching in the weak-field limit

In the perturbative limit, the integral in (3.9), with the polarization field $P_q(r, z)$ given by (3.14) can be performed analytically. The $q$th harmonic field $E_q$ is equal to (Ward and New 1969, Miles and Harris 1973, Bjorklund 1975)

$$E_q(r', z', t') = -i\pi k_q b \chi^q \mathcal{N}_0 E_0^q 2^{1-q} G_b^{q\omega}(r', z') \mathcal{G}_\tau^q(t') F_q(b, \Delta k). \tag{3.18}$$

$E_0$ is the peak laser intensity. $G_b^{q\omega}$ denotes a Gaussian beam envelope for a field oscillating at frequency $q\omega$, with wavevector $k_q$ and with a confocal parameter equal to $b$ (3.11). The generated harmonic field $E_q$ is Gaussian with the same confocal parameter and beam waist location as the fundamental field. Its focal section (equal to $\pi b/2k_q = b\lambda/4q$) decreases with increasing order. $\mathcal{G}_\tau^q$ is the $q$th power of the incident pulse distribution. The pulse width of the $q$th harmonic field is equal to $\tau/\sqrt{q}$ for a shaped (Gaussian) pulse, $\tau$ denoting the laser pulse width. Phase matching is described by the factor $F_q(b, \Delta k)$, defined by a one-dimensional integral over the non-linear medium as

$$F_q(b, \Delta k) = \int_{-\infty}^{+\infty} \exp\{-i[\{\Delta k z\} + (q-1)\tan^{-1}(2z/b)]\}$$

$$\times (1 + 4z^2/b^2)^{(1-q)/2} 2\rho(z) \, \mathrm{d}z/b \tag{3.19}$$

where $\rho(z) = \mathcal{N}(z)/\mathcal{N}_0$ is the atomic density distribution. The number of photons emitted at each laser shot is

$$N_q = \frac{\pi^2 b^3}{4\hbar} \tau_q \mathcal{N}_0^2 |\chi^q (E_0/2)^q|^2 |F_q(b, \Delta k)|^2 \tag{3.20}$$

where $\tau_q = \int_{-\infty}^{+\infty} \mathcal{G}_\tau^q(t) \, \mathrm{d}t$. Note that the single-atom response at the peak intensity $|d_q|^2 = |\chi^q(E_0/2)^q|^2$ and the effect of propagation in the medium, described by the dimensionless factor $|F_q(b, \Delta k)|^2$, can be factored out and are therefore independent, as long as the weak-field approximation remains valid.

We have studied the behaviour of $F_q(b, \Delta k)$ as a function of the process order $q$, the focusing geometry (characterized by the confocal parameter $b$) and also the phase mismatch $\Delta k$. The gas density distribution used in all the calculations presented in this paper is described by a truncated Lorentzian in the $z$-direction, $\rho(z) = 1/(1 + 4z^2/L^2)$ for $|z| \leq L$ and $\rho(z) = 0$ for $|z| > L$, with a width at half maximum of $L = 1$ mm. Figure 11($a$) shows the variation of $|F_q(b, \Delta k)|^2$ with the phase mismatch $\Delta k$ (assumed to be real) for the seventh harmonic and confocal parameters $b = 4$ mm, $b = 1$ mm, $b = 0.4$ mm. Figure 11($b$) shows $|F_q(b, \Delta k)|^2$ for $b = 1$ mm and $q = 3$, $q = 7$, $q = 13$. Although varying $b$ or $q$ leads of course to different results, the general trend is similar: as the process increases in order or as the geometry becomes more focused, the maximum of the phase-matching function shifts towards a higher negative phase
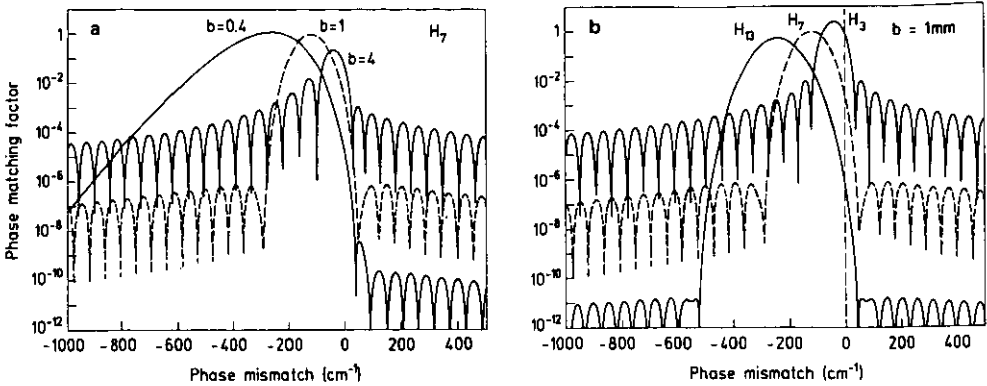
**Figure 11.** Phase matching factor $|F_q|^2$ as a function of the phase mismatch $\Delta k$ (cm$^{-1}$) in the perturbative limit. ($a$) 7th harmonic for $b = 4$ mm, $b = 1$ mm and $b = 0.4$ mm; ($b$) 3rd, 7th and 13th harmonics for $b = 1$ mm.

mismatch and the average level of the oscillations in the wings of $|F_q|^2$ decreases. These two effects are due respectively to the phase factor $[(q-1)\tan^{-1}(2z/b)]$ and to the amplitude term $(1 + 4z^2/b^2)^{(1-q)/2}$, induced by focusing.

Phase matching is optimized when the phase in (3.19) remains small. The optimum (negative) phase mismatch, which is close to $2(1 - q)/b$, increases with increasing order and decreasing confocal parameter (see figure 11). Indeed, the phase variation across the focus of the non-linear polarization induced by focusing becomes more rapid, leading to a larger phase lag between the generated field and its driving polarization. It must then be compensated by a greater phase mismatch $\Delta k$.

The amplitude factor in (3.19) affects the shape of $|F_q|^2$, particularly in the wings region. In the limit of an infinite medium and small coherence length, the harmonic fields generated before the focus are exactly cancelled by those created after the focus yielding no net harmonic generation. For a finite medium, exact cancellations occur only for some periodic values of the phase mismatch, which leads to oscillations in the wings of the phase matching function. The average level of these oscillations depends on how rapidly the amplitude term in (3.19) gets damped away from the focus. Therefore, it decreases as the geometry becomes more focused or, equivalently, as the process order increases. One might say that for the same confocal parameter of the incident beam, the interaction geometry becomes more and more of the tight focus type as the order of the harmonic increases.

The phase mismatch $\Delta k$ is proportional to the difference between the dynamic polarizabilities at the harmonic frequency and at the fundamental frequency: $\Delta k = 2\pi q\omega \mathcal{N}[\chi^1(-q\omega; q\omega) - \chi^1(-\omega; \omega)]/c$. We show in table 1 the values of the phase mismatch at 15 Torr $(5.3 \times 10^{17}$ atoms/cm$^3)$ in Xe for the harmonics emitted at multiples of the YAG frequency (L'Huillier *et al* 1990). By comparing these values with the horizontal scale in figure 11, one sees that perfect phase matching is not realized in the high-order harmonic generation experiments. In a first approximation, one can simply take the intersection of the functions plotted in figure 11($b$) with the line $\Delta k = 0$. $|F_q(b, \Delta k)|^2 \simeq |F_q(b, 0)|^2$. Since this is near the positive wing of $|F_q(b, \Delta k)|^2$, phase matching in the experimental conditions is essentially determined by the variation of the amplitude of the polarization field throughout the medium, and not so much by the variation of its phase. (As will be shown below, this conclusion will also be true

**Table 1.** Phase mismatches $(cm^{-1})^a$.

| | $q$ | | | | | | | | | |
|---|---|---|---|---|---|---|---|---|---|---|
| | 3 | 5 | 7 | 9 | 11 | 13 | 15 | 17 | 19 | 21 |
| Neutral Xe | 0.14 | 0.84 | 3.3 | 22 | ~5.7 | −14 | −19 | −22 | −23 | −24 |
| Free electrons[b] | 43 | 77 | 110 | 142 | 174 | 207 | 239 | 271 | 303 | 335 |

[a] At 15 Torr pressure.
[b] For a completely ionized medium.

in a strong-field situation.) In the weak-field limit the polarization field varies as the $q$th power of the incident field so that the volume in which the harmonics are generated becomes smaller as the process order increases. Phase matching is predicted to decrease with increasing order, leading to the expectation that any plateau in the single-atom response would be destroyed by propagation in a focused geometry.

As a further illustration, we show in figure 12 $|F_q(b, \Delta k)|^2$ as a function of the process order $q$ for the phase mismatches $\Delta k$ indicated in table 1 corresponding to the experimental conditions in xenon. Two geometries have been investigated: $b = 1$ mm (circles) and $b = 4$ mm (squares). The full curves indicate the weak-field limit calculations, the broken curves with symbols are strong-field calculations, which will be discussed later. The broken curves without symbols indicate the results obtained within the weak-field limit by neglecting dispersion $(\Delta k = 0)$. The comparison between $|F_q(b, \Delta k)|^2$ and $|F_q(b, 0)|^2$ for the two geometries shows that dispersion does not play an important role here, owing to the rather low pressure used in the experiments. In contrast, the effect of focusing leads to a substantial decrease of $|F_q(b, \Delta k)|^2$ with $q$, reflecting the fact that the polarization amplitude is more rapidly damped away from the focus. The importance of this effect increases as the laser is more strongly focused, as shown by comparing $|F_q(b = 1, \Delta k)|^2$ and $|F_q(b = 4, \Delta k)|^2$. Note in particular the twelve orders of magnitude difference between the 3rd and 25th harmonics in the tight focusing case.
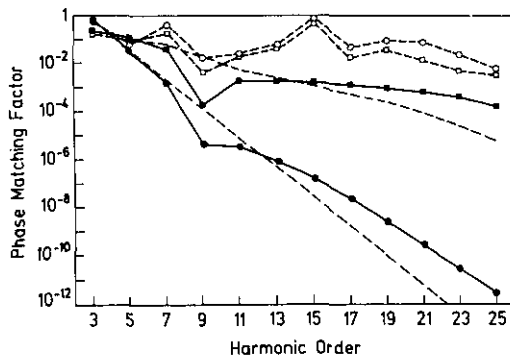


**Figure 12.** $|F_q(b, \Delta k)|^2$ as a function of the harmonic order $q$ in xenon at 15 Torr for two focusing geometries: $b = 1$ mm (circles) and $b = 4$ mm (squares). The perturbative results are shown by full curves, the non-perturbative results obtained at $3 \times 10^3$ W cm$^{-2}$ by broken curves with symbols. The broken curves without symbols indicate the perturbative results obtained by neglecting dispersion $(\Delta k = 0)$.

This weak-field analysis of the phase-matching conditions in the high-order harmonic generation experiments leads to the following conclusions: (i) phase matching decreases with increasing order, thus destroying any plateau observed in single-atom emission spectra; (ii) $|F_q(b, \Delta k)|^2$ varies with $b$ and this variation depends strongly on the process order $q$. Consequently, the harmonic signal $(b^3|F_q(b)|^2)$ should not have a simple $b^3$ scaling. These conclusions obviously contradict the experimental observations.

### 3.3. Phase matching in a strong-field regime

We now present our calculations of harmonic generation in a strong laser field. As explained in section 2.2, the single atom response, $d_q$, is obtained from the wavefunction generated by numerically integrating a time-dependent Schrödinger equation (Kulander and Shore 1989, 1990). We have concentrated our effort on the xenon atom, which has been experimentally investigated in great detail. In order to describe the non-linear polarization throughout the medium, i.e. for a distribution of intensities, we have calculated the $q$th component of the time-dependent dipole moment, $d_q$, over a fine intensity grid, between 0.5 and $5 \times 10^{13}$ W cm$^{-2}$ (assuming lowest-order perturbation theory to be valid below $5 \times 10^{12}$ W cm$^{-2}$).

The macroscopic parameters of the interaction are chosen to mimic the experimental conditions described in section 2.1. The incident laser beam is assumed to be Gaussian and we consider two cases with confocal parameters $b = 4$ mm or $b = 1$ mm (equation 3.11)). The laser pulse shape is taken to be Gaussian with a 36 ps width at half maximum. The phase mismatch ($\Delta k$) is assumed to be intensity independent and is given in table 1.

So far, harmonic generation has been discussed for a neutral medium. In the experiments described in section 2, the effect of ionization becomes significant above $2 \times 10^{13}$ W cm$^{-2}$ and therefore needs to be included. We account for the depletion of the neutral medium by using ionization rates obtained from the same non-perturbative time-dependent calculations. In (3.14), $\mathcal{N}(z)$ is replaced by

$$\mathcal{N}(r, z, t) = \mathcal{N}(z) \exp\left( - \int_{-\infty}^{t} p(r, z, t')\, dt' \right) \tag{3.21}$$

$p(r, z, t)$ denoting the ionization rate calculated at the intensity $I(r, z, t)$. (Here, the time $t$ is related to the slow temporal variation of the fields.) We neglect any contribution to the polarization field from ions, because it is expected to be smaller than the atomic one. The presence of free electrons introduces a space- and time-dependent change of the refractive index of the medium. The index at frequency $q\omega$ becomes $n_q + \Delta n_q^e(r, t)$, with $\Delta n_q^e(r, t) = -\omega_p^2/2q^2\omega^2$, where $\omega_p^2 = 4\pi\mathcal{N}_e(r, t)e^2/m$ is the square of the plasma frequency and $\mathcal{N}_e(r, t)$ denotes the electron density. It reduces the efficiency of the frequency conversion, introducing an additional positive phase mismatch between the harmonic field and its driving polarization: $\Delta k_q^e(r, t) = (\Delta n_q^e - \Delta n_1^e)q\omega/c = 2\omega_p^2(q^2 - 1)/qc\omega$. The values of $\Delta k_q^e$ for a completely ionized medium ($\mathcal{N}_e = \mathcal{N}_0 = 5.3 \times 10^{17}$ atoms/cm$^3$) are much more important than the phase mismatches due to the dispersion in the neutral medium, as shown in table 1. As soon as the intensity is high enough for a few per cent of the atoms to be ionized, dispersion is dominated by the presence of electrons. We have tried to estimate this effect by adding to the usual (atomic) phase mismatch $\Delta k$ the one induced by the presence of free electrons created by multiphoton ionization, which we assume to be motionless during the pulse time.

This is of course not valid for a 40 ps pulse, but it gives an upper estimate of the free electrons, influence. As already pointed out in section 3.1, we also neglect the defocusing effect that these free electrons might have on the propagating fields, considering only the variation of the phase mismatch.

The number of photons emitted at a given harmonic frequency is obtained by calculating the generated field $E_q(r', t')$ (with $t' - t \approx (z' - z)/c$) and then by integrating temporally and spatially the intensity profile $|E_q(r', t')|^2$. The results of our calculations in xenon for several laser intensities ranging from $5 \times 10^{12}$ W cm$^{-2}$ to $3 \times 10^{13}$ W cm$^{-2}$ and for a $b = 4$ mm laser confocal parameter are shown in figure 13. They can be compared with the experimental results in absolute value (figure 3) and also with single atom emission spectra (figure 8). At the highest laser intensity $3 \times 10^{13}$ W cm$^{-2}$, where ionization becomes significant, we show results obtained with and without including *the effect of free electrons (plotted respectively with stars and open circles). Although* the additional positive phase mismatch induced by these free electrons is large, especially for the high harmonics, the resulting decrease in efficiency remains weak, at most a factor of two, and sometimes non-existent.
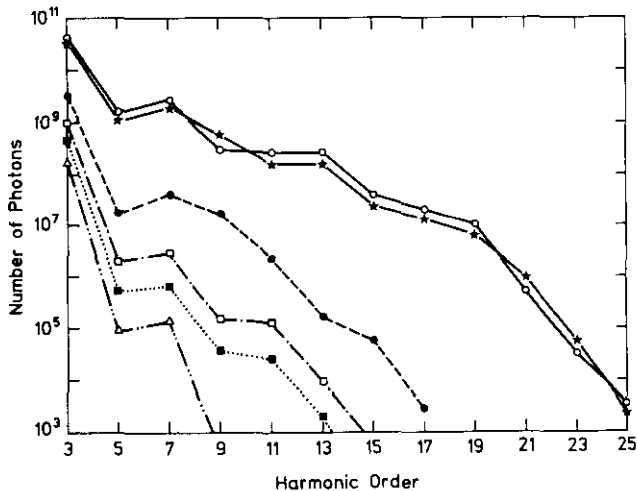


**Figure 13.** Calculated number of photons for $b = 4$ mm, $L = 1$ mm at the same laser intensities as in figure 3 (L'Huillier *et al* 1991c).

The theoretical curves are generally higher than the experimental results particularly for the highest intensity. They are, however, mostly within the experimental error bar, estimated to be one order of magnitude. The general behaviour of the harmonic spectrum as a function of the laser intensity is well reproduced. The effect of phase matching is seen to be most important at the lowest intensity, i.e. in the weak-field limit. High harmonics are not as well phase matched as low-order ones. At the lowest *intensity, the cutoff occurs at a much lower order* (9 instead of 15) in the many-atom response than in the single-atom response (compare figures 8 and 13). However, at laser intensities above $9 \times 10^{12}$ W cm$^{-2}$, the length of the plateau is quite similar to that of the single-atom response (see figure 8), as if all the harmonics were equally phase matched. From the lowest intensity to about $10^{13}$ W cm$^{-2}$ (below the onset of saturation), the number of photons rises more rapidly with the laser intensity than $|d_q|^2$: the effects of imperfect phase matching are lessening with increasing laser intensity.

The dotted curve in figure 4, which was presented in section 2, shows the result of our calculation for the 15th harmonic. There is a disagreement of a factor of two between the calculated and experimental saturation intensities and of a factor of seven for the harmonic signal. However, the relative agreement between both results is remarkable (see the full curve). Our calculation can reproduce fairly well the behaviour of the saturation, which is mainly due to depletion, and also the high power law ($\sim I^{11}$) below the onset of saturation. This power law is higher than the one obtained in the single atom response, again indicating a substantial improvement of phase matching conditions as the intensity increases and as one departs from the weak-field limit.

Similar results as those presented in figure 13 have been obtained with a tighter focusing geometry ($b = 1$ mm). The calculations show the same $b^3$ scaling that was observed in the experiments (see section 2.4). The shape of the harmonic distribution at high intensity is relatively insensitive to the geometry, in contrast to the weak-field limit predictions discussed previously.

Some information can also be gained by studying the spatial and temporal profiles of the generated fields, which have not been measured experimentally so far. Figure 14($a$) presents the spatial profile in the far field of the 15th harmonic in a strong field situation at $3 \times 10^{13}$ W cm$^{-2}$. Here, for simplicity, we exclude the effect of free electrons and we take a 'snapshot' of the profile at the maximum of the pulse at time $t = 0$. The results are shown for two focusing geometries, collimated ($b = 4$ mm, broken curve) and confocal ($b = 1$ mm, chain curve). All the profiles have been normalized to unity at the maximum. The horizontal scale has been chosen so that the perturbative Gaussian profiles corresponding to the two geometries, which are shown by the full curve in the figure, be superposed. At high laser intensity, for $b = 4$ mm, the far-field harmonic profile becomes narrower, which means that the harmonic beam is defocused compared with the perturbative limit. Rings appear, particularly in the tight focus geometry. However, the integrated signal does not depend strongly on how the energy is spatially distributed. In the perturbative limit, the high harmonics become more focused with increasing order (focal section varying in $1/q$). By contrast, in the strong-field regime, their focal section remains approximately constant for the harmonics of the plateau region.

We have also studied the temporal profiles of the harmonics, obtained by integrating the spatial distributions $[\int |E_q(r', t')|^2 r' \, dr']$. These profiles, which are quite insensitive to the geometry, are generally larger than in the weak-field limit. They are of the order of 15 ps for the plateau harmonics for a 36 ps incident laser pulse. Figure 14($b$) shows the temporal intensity profile of the 15th harmonic at $b = 1$ mm and $3 \times 10^{13}$ W cm$^{-2}$. The asymmetry of the profile arises from the depletion of the population of neutral atoms during the pulse, which reduces the conversion efficiency for positive times (at the end of the pulse).

Finally, we found it useful for a better understanding of these results to separate the role of propagation from the single atom contribution in the calculations, as we did in the perturbative case. We define $|F_q(b, \Delta k)|^2$ by analogy with equation (3.19) as

$$|F_q(b, \Delta k)|^2 = \frac{4\hbar N_q}{\pi^2 b^3 \tau_q \mathcal{N}_0^2 |d_q|^2} \tag{3.22}$$

where $|d_q|^2$ denotes the dipole moment evaluated at the maximum intensity of the pulse (at best focus). Note that, in this definition, $|F_q(b, \Delta k)|^2$ not only characterizes the coherence length of the process but also reflects the spatial (and temporal) profile of the emitted harmonics in comparison with the weak-field limit. Here we assume a
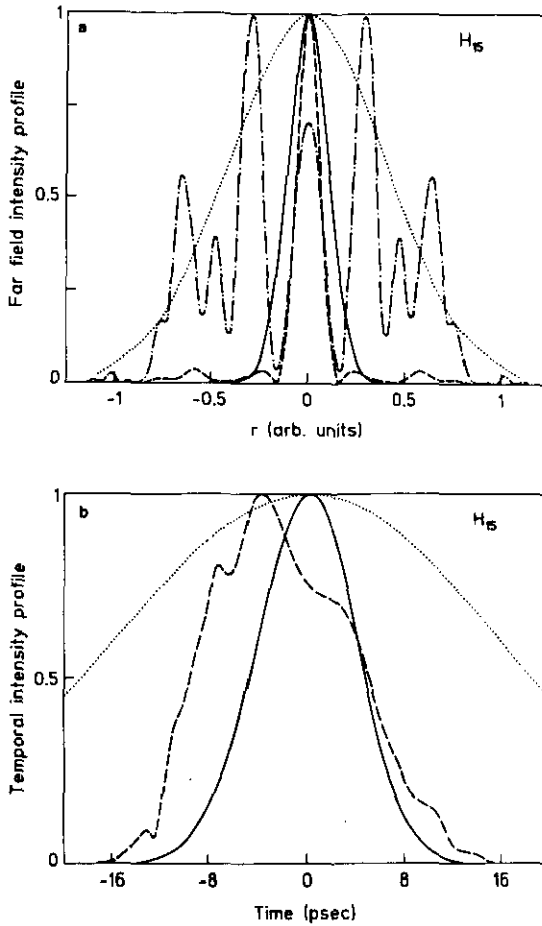
**Figure 14.** Fifteenth harmonic intensity temporal and far field profiles at $3 \times 10^{13}$ W cm$^{-2}$. The envelope shown by the dotted curve indicates the incident laser profile. ($a$) Spatial profile for $b = 1$ mm (chain curve) and $b = 4$ mm (broken curve). ($b$) Temporal profile for $b = 1$ mm.

square laser pulse which is short enough for ionization to be negligible (so that the separation of the single-atom response and propagation remains meaningful). The broken curves at the top in figure 12 (see section 3.2) show the phase matching factor $|F_q(b, \Delta k)|^2$ at $3 \times 10^{13}$ W cm$^{-2}$. Although in the weak-field limit $|F_q(b, \Delta k)|^2$ decreases rapidly with increasing order, and is strongly dependent on the geometry, in contrast, at $3 \times 10^{13}$ W cm$^{-2}$, $|F_q(b, \Delta k)|^2$ remains between 1 and $10^{-2}$, independent of the order. Moreover, it is relatively insensitive to the geometry. Our calculations yield results that are indeed in good agreement with the experimental conclusions and in strong disagreement with the weak-field predictions.

## 3.4. Interpretation

We now try to explain why going to a strong-field regime for the laser–atom interaction significantly improves the phase matching of the high harmonics. Compared with a

perturbative picture, the dipole moment $d_q$ obtained from the time-dependent calculation (or from any non-perturbative method) varies generally less rapidly with the laser intensity and similarly for most of the harmonics (which gives rise to the plateau behaviour). It shows structures and resonances (see figure 9). Finally, it has an intensity-dependent phase lag relative to the fundamental. What influences phase matching is the first property, namely the fact that the dependence of the dipole moment on the electric field is (on average) much weaker than that predicted within lowest-order perturbation theory. In order to illustrate this idea and to get some insight into the reason why the high harmonics are phase matched in the same way, we shall now consider a simple model: we assume that the dipole moment $d_q$ varies as the $p$th power of the incident laser field, $p$ denoting an effective order of non-linearity, lower than the harmonic order $(d_q(r, z) = \zeta_q |E_1(r, z)|^p)$. As in the perturbative limit, the integral in (3.9) can be performed partly analytically, though the expressions are more cumbersome. The harmonic field can be written as (L'Huillier *et al* 1991b)

$$E_q(r', z') = -2i\pi k_q b \zeta_q \mathcal{N}_0 E_0^p \mathscr{F}_q(r', z') \tag{3.23}$$

with

$$\mathscr{F}_q(r', z') = \int_{-\infty}^{+\infty} \frac{\exp[-k_q r'^2/b''\alpha(z, z')]}{\alpha(z, z')} \exp[-i\{\Delta k z\} - iq \tan^{-1}(2z/b) + i \tan^{-1}(2z/b')]$$
$$\times (1+4z^2/b^2)^{(2-p)/2}(1+4z^2/b'^2)^{-1/2} 2\rho(z) \, dz/b. \tag{3.24}$$

We have introduced the notations

$$b' = pb/q \qquad b'' = qb/p \qquad \alpha(z, z') = (1+4z^2/b^2)/(1-2iz/b') + 2i(z'-z)/b''.$$

$|F_q(b, \Delta k)|^2$ is defined by

$$|F_q(b, \Delta k)|^2 = \frac{4k_q}{b} \int |\mathscr{F}_q(r', z')|^2 r' \, dr'. \tag{3.25}$$

In the loose focusing limit $(b \gg L)$, $\alpha(z, z')$ reduces to $1 + 2iz'/b''$. The first term in the integrand of (3.24) is the Gaussian distribution $G_{b''}^{qw}(r', z')$, which can be taken out of the $z$-dependent integral. The generated harmonic field $E_q$ is therefore Gaussian with a confocal parameter $b''$ larger than that predicted in the weak-field limit. The focal section of the generated beam, equal to $\pi b''/2k_q = b\lambda/4p$ depends on the effective order $p$, rather than on the non-linear order $q$. The rest of the integral is quite close to (3.19), apart from the amplitude term, which varies approximately as $(1 + 4z^2/b^2)^{(1-p)/2}$, instead of $(1+4z^2/b^2)^{(1-q)/2}$. When $p \ll q$, this term varies much less rapidly throughout the medium than in the perturbative limit. As discussed previously, phase matching around $\Delta k = 0$ is determined by the variation of the polarization *amplitude* throughout the medium. It depends on the effective order of non-linearity $(p)$ of the dipole moment $d_q$. Therefore it remains relatively constant for all the harmonics which have the same intensity dependence.

In a more general case, the generated harmonic field is not Gaussian. The situation is quite similar to difference-frequency processes (Bjorklund 1975). The term $\exp[-k_q r'^2/b''\alpha(z, z')]$ leads to a strong distortion of the spatial profile which develops rings. From (3.24), one sees that phase matching can be favoured for some $r'$ values, which may be different from zero (off axis). The number of these rings increases as the geometry becomes more focused. Typically, for $b = 4$ mm, there is a central spot and an external ring, whereas for $b = 1$ mm, up to four or five rings may appear (see

figure 14($a$)). Although phase matching in this case cannot be reduced to a one-dimensional problem along the propagation axis, the conclusion reached in the loose focusing case remains also valid: since phase matching depends on the variation of the amplitude of the polarization field throughout the medium which does not depend on the process order, it remains constant for all the harmonics in the plateau. Figure 15 compares $|F_q(b, \Delta k)|^2$ for the 5th, 13th and 21st harmonics in the weak-field limit (full curve) and for the 13th and 21st harmonics in the model situation where $|d_q|^2$ is assumed to vary with the laser field strength as $|E_1|^5$. At $\Delta k = 0$, $|F_q(b, 0)|^2$ remains relatively constant for the model harmonics, whereas it decreases rapidly with $q$ in the perturbative limit.
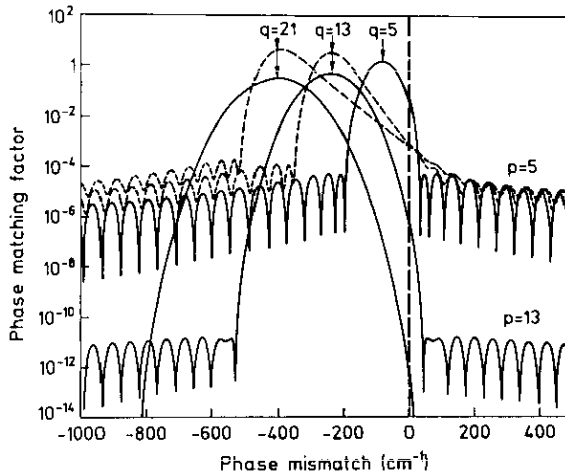


**Figure 15.** Phase matching factor $|F_q|^2$ for the 5th, 13th and 21st harmonics as a function of the phase mismatch $\Delta k$ (cm$^{-1}$) for $b = 1$ mm and $L = 1$ mm. The full curves indicate the perturbative results. The broken curves are results obtained by assuming a fifth power dependence for the 13th and 21st harmonics.

This simple model, which can be carried out analytically for the most part, reproduces fairly well the main aspects of the numerical calculation using as a source the non-perturbative atomic dipole moment. It shows that the main difference between the strong- and weak-field regimes is the rate at which the magnitude of the polarization field varies within the medium. This has an important effect on the conversion efficiency because, in the experimental conditions, phase matching does not depend much on the *phases* of the interfering fields, but it does depend on the variation of the *amplitudes* of the fields throughout the medium. In a strong-field regime, the harmonics get defocused compared with the perturbative limit and, moreover, the phase matching is found to be relatively constant with increasing order.

## 4. Conclusion

As was pointed out in the introduction, these harmonic generation processes are difficult to grasp because of the interplay between the microscopic response (emission of

harmonics by a single atom) and the collective one (propagation, phase matching of the propagating fields). In conclusion, we would like to summarize the role played by the many parameters of the problem, related either to the pump field or to the non-linear medium, influencing either the atomic response or propagation, or both. These must be viewed as a few tentative guidelines, most of them requiring a more thorough investigation, rather than definite conclusions.

*Laser intensity.* As the incident pump intensity increases, the plateau increases rapidly both in length and in amplitude, because these processes are highly non-linear. This remains true up to the intensity at which the atoms are depleted by ionization.

*Laser pulse length.* Shortening the pulse length increases the intensity at which the atoms are ionized. Consequently, the medium can produce more harmonics because it can experience a higher intensity. Note that the pulse length of generated radiation follows that of the pump field, being smaller by about a factor of two.

*Laser wavelength.* This aspect has not been discussed in this paper where we have focused on the results at 1 $\mu$m. On the basis of experiments at 248 nm (McPherson *et al* 1987) and calculations of single atom spectra performed at 532 nm and 1064 nm (Potvliege and Shakeshaft 1989b, Krause *et al* 1991), one might expect the harmonic conversion efficiency to increase for shorter incident wavelengths and the plateau to remain approximately of the same length in photon energy.

*Laser confocal parameter.* This provides a simple way of increasing the harmonic generation efficiency, which was found to vary as $b^3$, in the range $b = 1$-$6$ mm and $L = 1$ mm. Note that in the plane-wave limit the $b$-scaling should become less rapid, being approximately linear.

*Atom.* Atoms with higher ionization energies can produce more harmonics but with a reduced efficiency. A still open question is whether ions can efficiently produce harmonics.

*Atomic density.* The signal varies as $\mathcal{N}^2$ independent of the order. This is true between 1 and 25 Torr at 1 $\mu$m. Saturation effects (Rosman *et al* 1988) are to be expected for shorter incident wavelengths and higher gas pressures.

Finally, let us emphasize the main conclusion reached in this paper. These high-order harmonic generation processes are twice the signature of a strong-field interaction with a non-linear medium, which cannot be described using weak-field approximations. The emission of radiation by a single atom has a non-perturbative behaviour: it exhibits the same plateau that was observed in the experiments; the harmonics do not vary as $I^q$, where $q$ is the process order. Moreover, the plateau is conserved in the many-atom response, a fact that cannot be reconciled with a weak-field approach to the problem. It comes from the variation of the non-linear polarization with the laser intensity which is lower than in the weak-field limit and also similar for all the harmonics in the plateau. Extending harmonic generation into a strong-field regime has two unexpected and fortunate consequences: a plateau forms in the single-atom response, which means that generation of, say, the 17th harmonic is as probable as the generation of the 5th harmonic; and all the generated harmonics become equally and efficiently phase matched.

part under the auspices of the Department of Energy at the Lawrence Livermore National Laboratory under contract number W-7405-Eng-48.

*Note added in proof.* The laser focal section obtained with the $f = 200$ mm lens has been recently measured and has been found to be about a factor of two smaller than the one estimated previously. This does not change any of the conclusions of the paper but leads to a better agreement between the calculated saturation intensity and the experimental one (increased by a factor of two) and also between the calculated and measured numbers of harmonic photons.

# References

Akhmanov S A, Khokhlov R V and Sukhorukov A P 1972 *Laser Handbook* ed F T Arecchi and E O Schulz-Dubois (Amsterdam: North-Holland)
Arkhipkin V G and Popov A K 1987 *Sov. Phys.-Usp.* **30** 952-76 (*Usp. Fiz. Nauk.* **153** 423-68)
Bandarage G, Maquet A and Cooper J 1990 *Phys. Rev.* A **41** 1744-6
Becker W, Long S and McIver J K 1990 *Phys. Rev.* A **41** 4112-5
Bishop D M and Lam B 1988 *Phys. Rev.* A **37** 464-9
Biedenharn L C, Rinker G A and Solem J C 1989 *J. Opt. Soc. Am.* **6** 221-7
Bjorklund G C 1975 *IEEE J. Quantum Electron.* **QE-11** 287-96
Bloembergen N 1965 *Nonlinear Optics* (New York: Benjamin)
Bokor J, Bucksbaum P H and Freeman R R 1983 *Opt. Lett.* **8** 217-9
Chu S I, Wang K and Layton E 1990 *J. Opt. Soc. Am.* B **7** 425-32
Delone N B and Krainov V P 1988 *Fundamentals of Nonlinear Optics of Atomic Gases* (New York: Wiley)
DeVries P L 1990 *J. Opt. Soc. Am.* B **7** 517-20
Drabovich K N, Kulagin I A and Usmanov T 1985 *Sov. J. Quantum Electron.* **15** 402-4 (*Kvant. Elektron.* **12** 616-9)
Eberly J H, Su Q and Javanainen J 1989a *Phys. Rev. Lett.* **62** 881-4
—— 1989b *J. Opt. Soc. Am.* B **6** 1289-98
Eberly J H, Su Q, Javanainen J, Kulander K C, Shore B W and Roso-Franco L 1989c *J. Mod. Opt.* **36** 829-53
Ferray M, L'Huillier A, Li X F, Lompré L A, Mainfray G and Manus C 1988 *J. Phys. B: At. Mol. Opt. Phys.* **21** L31-5
Ganeev R A, Gorbushin I A, Kulagin I A and Usmanov T 1985 *Opt. Spectrosc.* **61** 807-8
Gao B and Starace A F 1989 *Phys. Rev.* A **39** 4550-60
Grischkowsky D 1970 *Phys. Rev. Lett.* **24** 866-9
Groseva M G, Metchkov D I, Mitev V M, Pavlov L I and Stamenov K V 1977 *Opt. Commun.* **23** 77-9
Gontier Y and Trahin M 1982 *IEEE J. Quantum Electron.* **QE-18** 1137-45
Hanna D C, Yuratich M A and Cotter D 1979 *Nonlinear Optics of Free Atoms and Molecules* (Berlin: Springer)
Jackson J D 1975 *Classical Electrodynamics* 2nd edn (New York: Wiley)
Kildal H and Brueck S R J 1980 *IEEE J. Quantum Electron.* **QE-16** 566-73
Kleinman D A 1962 *Phys. Rev.* **128** 1761-75
Krause J L, Schafer K J and Kulander K C 1991 *Phys. Rev.* A in press
Kulander K C and Rescigno T N 1991 *Comput. Phys. Commun.* **63** 523-8
Kulander K C and Shore B W 1989 *Phys. Rev. Lett.* **62** 524-6
—— 1990 *J. Opt. Soc. Am.* B **7** 502-8
Kung A H 1983 *Opt. Lett.* **8** 24-6
LaGattuta K J 1990 *Phys. Rev.* A **41** 5110-6
Lago A, Hilber G and Wallenstein R 1987 *Phys. Rev.* A **36** 3827-36
L'Huillier A, Li X F and Lompré L A 1990 *J. Opt. Soc. Am.* B **7** 527-36
L'Huillier A, Lompré L A, Ferray M, Li X F, Mainfray G and Manus C 1988 *Europhys. Lett.* **5** 601-5
L'Huillier A, Lompré L A, Mainfray G and Manus C 1991a *Proc. 5th Int. Conf. on Multiphoton Processes (Paris)*
—— 1991b *Adv. At. Mol. Opt. Phys.* in press
L'Huillier A, Schafer K J and Kulander K C 1991c *Phys. Rev. Lett.* **66** 2200-3
Lompré L A, Ferray M, L'Huillier A, Li X F and Mainfray G 1988 *J. Appl. Phys.* **63** 1791-3
Lompré L A, L'Huillier A, Monot P, Ferray M, Mainfray G and Manus C 1990 *J. Opt. Soc. Am.* **7** 754-61
Li X F, L'Huillier A, Ferray M, Lompré L A and Mainfray G 1989 *Phys. Rev.* A **39** 5751-61

Mahon R and Yiu Y M 1980 *Opt. Lett.* **5** 278–80

Malcuit M S, Boyd R W, Davis W V and Rzazewski K 1990 *Phys. Rev.* A **41** 3822–5

Manakov N L and Ovsyannikov V D 1980 *Sov. Phys.–JETP* **52** 895–900 (*Zh. Eksp. Teor. Fiz.* **79** 1769–78)

Manakov N L, Ovsyannikov V D and Rapoport L P 1975 *Sov. J. Quantum Electron.* **5** 22–6 (*Kvant. Elektron.* **2** 43–50)

Marburger J H 1975 *Prog. Quantum Electron.* **4** 35–110

McPherson A, Gibson G, Jara H, Johann U, Luk T S, McIntyre I, Boyer K and Rhodes C K 1987 *J. Opt. Soc. Am.* B **4** 595–601

Metchkov D I, Mitev V M, Pavlov L I and Stamenov K V 1977 *Opt. Commun.* **21** 391–4

Miles R B and Harris S E 1973 *IEEE J. Quantum Electron.* **QE-9** 470–84

Miyazaki K and Kashiwagi H 1978 *Phys. Rev.* A **18** 635–43

Pan L, Taylor K T and Clark C W 1989 *Phys. Rev.* A **39** 4894–7

—— 1990 *J. Opt. Soc. Am.* B **7** 509–16

Potvliege R M and Shakeshaft R 1989a *Z. Phys.* D **11** 93–4

—— 1989b *Phys. Rev.* A **40** 3061–79

Puell H, Spanner K, Falkenstein W, Kaiser W and Vidal C R 1976 *Phys. Rev.* A **14** 2240–57

Reintjes J 1984 *Nonlinear Optical Parametric Processes in Liquids and Gases* (New York: Academic)

Reintjes J, She C Y and Eckardt R C 1978 *IEEE J. Quantum Electron.* **QE-14** 581–96

Reintjes J, Tankersley L L and Christensen R 1981 *Opt. Commun.* **39** 334–8

Rettner C T, Marinero E E, Zare R N and Kung A K 1984 *J. Phys. Chem.* **88** 4459–65

Rosman R, Gibson G, Boyer K, Jara H, Luk T S, McIntyre I A, McPherson A, Solem J C and Rhodes C K 1988 *J. Opt. Soc. Am.* B **5** 1237–42

Sacks R A and Szöke A 1991 *J. Opt. Soc. Am.* B in press

Sarukura N, Hata K, Adachi T, Nodomi R, Watanabe M and Watanabe S 1991 *Phys. Rev.* A **43** 1669–72

Shen Y R 1984 *The Principles of Nonlinear Optics* (New York: Wiley)

Shore B W and Knight P L 1987 *J. Phys. B: At. Mol. Phys.* **20** L413–23

Shore B W and Kulander K C 1989 *J. Mod. Opt.* **36** 857–75

Sitz P and Yaris R 1968 *J. Chem. Phys.* **49** 3546–57

Sundaram B and Milonni P W 1990 *Phys. Rev.* A **41** 6571–3

Tomov I V and Richardson M C 1976 *IEEE J. Quantum Electron.* **QE-12** 521–31

Varga R S 1962 *Matrix Iterative Analysis* (Englewood Cliffs, NJ: Prentice-Hall)

Ward J F and New G H C 1969 *Phys. Rev.* A **185** 57–72

Wildenauer J 1987 *J. Appl. Phys.* **62** 41–8

Zych L J and Young J F 1978 *IEEE J. Quantum Electron.* **QE-14** 147–9